

# Interactions between Signal-Transducing Proteins Measured by Atomic Force Microscopy

Il Hong Kim,<sup>†</sup> Hye Young Lee,<sup>‡,||</sup> Hae Dong Lee,<sup>†,⊥</sup> Yu Jin Jung,<sup>†,#</sup> Saul J. B. Tandler,<sup>§</sup> Philip M. Williams,<sup>§</sup> Stephanie Allen,<sup>§</sup> Sung Ho Ryu,<sup>‡</sup> and Joon Won Park<sup>\*,†</sup>

National Core Research Center for Systems Bio-Dynamics, Department of Chemistry, Department of Life Science, Pohang University of Science and Technology, San 31 Hyoja-dong, Pohang, 790-784, Korea, and Laboratory of Biophysics and Surface Analysis, School of Pharmacy, The University of Nottingham, Nottingham NG7 2RD, U.K.

Atomic force microscopy (AFM) has been used to study the specific interactions between the signal-transducing proteins mammalian phospholipase D1 (PLD1), phospholipase C- $\gamma$ 1 (PLC- $\gamma$ 1), and Munc-18-1. To record the forces between them, the Phox homology (PX) domain of PLD1, the Src homology (SH3) domain of PLC- $\gamma$ 1, and Munc-18-1 were fused with glutathione S-transferase (GST) and immobilized onto reduced glutathione (GSH)-tethered surfaces. In order to enhance the recognition efficiency and avoid undesirable complications, both AFM tips and substrates were first modified with dendrons of two different sizes. Under the employed conditions, the probability of observing an unbinding event increased, most force–distance curves showed the single rupture events, and the unbinding forces were  $51 \pm 2$  pN for PX–(Munc-18-1) and  $42 \pm 2$  pN for PX–SH3. To investigate dynamics of these biomolecular interactions, we measured the loading rate dependence of the unbinding forces. The unbinding forces increased linearly with the logarithm of the loading rate, indicating the presence of a single potential barrier in the dissociation energy landscape. The measured off-rate constants ( $k_{\text{off}}$ ) at 15 °C were  $10^{-3.4 \pm 0.3} \text{ s}^{-1}$  for PX–(Munc-18-1) and  $10^{-1.7 \pm 0.1} \text{ s}^{-1}$  for PX–SH3. Further, we elucidated the influence of free SH3 and Munc-18-1 on the specific PX–(Munc-18-1) and PX–SH3 interaction, respectively.

Experimental analysis of biological systems by conventional methods such as immunoassay,<sup>1</sup> chromatography,<sup>2</sup> and isothermal titration calorimetry<sup>3</sup> is informative and useful but partly limited

by taking averages of molecular ensembles. This is particularly problematic when information about the behavior of an individual molecule is required. The limitation imposed on the analysis can be overcome by the measurement at a single molecular level. As an example, ensemble studies of myosin motors obtained using conventional methods suggested a simplified model for the mechanical and biochemical events. In the 1990s, as the single molecular detection techniques were developed, the movements of single myosin molecules along the actin filaments, concurrent with ATP hydrolysis, were elucidated in detail. These studies revealed that myosin moved backward in some cases and that the movement could be even be delayed up to 2 s after ADP departed from the myosin binding domain.<sup>4–6</sup> Single-molecule methods therefore provided information about myosin motors that had never been elucidated from experiments on molecular ensembles, illustrating that they were essential in understanding molecular motors precisely.

Atomic force microscopy (AFM) is an excellent tool to image a surface at high resolution<sup>7</sup> and to detect and measure the interaction within or between biomolecules.<sup>8–11</sup> Because it is possible to measure interaction force as low as the piconewton range, AFM is becoming a rapidly developing technique for probing affinity and recognition properties at the single molecular level, and compared to other sensitive methods for force measurement, the AFM shows high force resolution and the ability to be operated under physiological condition for studying specific interactions between DNA–DNA,<sup>8,11</sup> antigen–antibody,<sup>10</sup> and aptamer–protein.<sup>12</sup>

Mammalian phospholipase D (PLD) is a membrane-bound enzyme that generates a multifunctional lipid second messenger,

\* To whom correspondence should be addressed. E-mail: jwpark@postech.ac.kr. Phone: +82-54-279-2119. Fax: +82-54-279-0653.

<sup>†</sup> Department of Chemistry, Pohang University of Science and Technology.

<sup>‡</sup> Department of Life Science, Pohang University of Science and Technology.

<sup>§</sup> The University of Nottingham.

<sup>||</sup> Current address: Department of Physiology, University of California, San Francisco, California 94158.

<sup>⊥</sup> Current address: Korea Institute of Construction Materials, 14-1 Dang-dong, Gunpo, 405-010, Korea.

<sup>#</sup> Current address: Department of Cellular Machines, University of Technology Dresden, Tatzberg 49, D-01307 Dresden, Germany.

(1) Chu, K. S.; Jin, G.; Guo, J. R.; Ju, M.; Huang, J. J. *Biotechnol. Prog.* **1995**, *11*, 352–356.

(2) Ishiwata, N.; Takio, K.; Katayama, M.; Watanabe, K.; Titani, K.; Ikeda, Y.; Handa, M. *J. Biol. Chem.* **1994**, *269*, 23708–23715.

(3) Wiseman, T.; Williston, S.; Brandts, J. F.; Lin, L.-N. *Anal. Biochem.* **1989**, *179*, 131–137.

(4) Finer, J. T.; Simmons, R. M.; Spudich, J. A. *Nature (London)* **1994**, *368*, 113–119.

(5) Funatsu, T.; Harada, Y.; Tokunaga, M.; Saito, K.; Yanagada, T. *Nature (London)* **1995**, *374*, 555–559.

(6) Kitamura, K.; Tokunaga, M.; Iwane, A. H.; Yanagida, T. *Nature (London)* **1999**, *377*, 129–134.

(7) Engel, A.; Müller, D. J. *Nat. Struct. Biol.* **2000**, *7*, 715–718.

(8) Strunz, T.; Oroszlan, K.; Schäfer, R.; Güntherodt, H.-J. *Proc. Natl. Acad. Sci. U.S.A.* **1999**, *96*, 11277–11282.

(9) Oberhauser, A. F.; Marszalek, P. E.; Carrion-Vazquez, M.; Fernandez, J. M. *Nat. Struct. Biol.* **1999**, *6*, 1025–1028.

(10) Schwesinger, F.; Ros, R.; Strunz, T.; Anselmetti, D.; Güntherodt, H.-J.; Honegger, A.; Jermutus, L.; Tiefenauer, L.; Plückthun, A. *Proc. Natl. Acad. Sci. U.S.A.* **2000**, *97*, 9972–9977.

(11) Jung, Y. J.; Hong, B. J.; Zhang, W.; Tandler, S. J. B.; Williams, P. M.; Allen, S.; Park, J. W. *J. Am. Chem. Soc.* **2007**, *129*, 9349–9355.

(12) Jiang, Y.; Zhu, C.; Ling, L.; Wan, L.; Fang, X.; Bai, C. *Anal. Chem.* **2003**, *75*, 2112–2116.

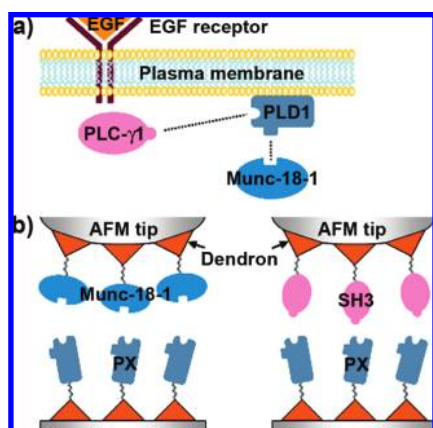


**Figure 1.** (a) Model of signal-transducing proteins. (b) Schematic drawing of GST-fused Munc-18-1 and GST-fused SH3 immobilized onto the dendron-modified AFM tip, and GST-fused PX immobilized onto the dendron-modified substrate through GSH–GST interaction.

phosphatidic acid (PA), in response to a variety of signals, including hormones, neurotransmitters, and growth factors.<sup>13</sup> In particular, epidermal growth factor (EGF) stimulation has been known to increase PLD activity and is involved in cellular functions. Recently, two molecules, phospholipase C-γ1 (PLC-γ1) and Munc-18 have been reported as the EGF-dependent regulators of PLD through Phox homology (PX) domain (Figure 1a),<sup>14,15</sup> but their detailed relationship has not been revealed yet. The enzymatic activity of PLC-γ1, a downstream signaling component of EGF, is required for the EGF-induced cellular responses.<sup>16–18</sup> It has been suggested that interaction between the Src homology (SH3) domain of PLC-γ1 and PX domain of PLD is important for the proper activation of PLC-γ1 after EGF stimulation.<sup>14,15</sup> Munc-18-1 was originally identified as a major brain protein, which binds to syntaxin, a synaptic vesicle fusion protein.<sup>19–21</sup> Recent report suggested that Munc-18-1 is also involved in EGF signaling.<sup>15</sup> Munc-18-1 binds to the PX domain of PLD and inhibits the basal PLD activity, but after EGF treatment, Munc-18-1 dissociates from PLD to activate PLD. In this model, PLC-γ1 has been suggested as a competitive factor because PLC-γ1 interacts with the PX domain of PLD in an EGF-dependent manner.

In this study, we used AFM to understand quantitatively the interactions between signal-transducing proteins, Munc-18-1, PLD1, and PLC-γ1 at a single-molecule level. To record the force between them, the PX domain of PLD1, the SH3 domain of PLC-γ1, and Munc-18-1 were specifically fused with glutathione

S-transferase (GST), and the GST-fused proteins were immobilized onto a reduced glutathione (GSH)-tethered surface. In order to enhance the recognition efficiency and avoid undesirable multiple interactions, both AFM tip and substrate were modified with one of two different size dendron species (Figure 1b). The effectiveness of the dendron approach has been demonstrated with DNA–DNA force measurement<sup>11</sup> and imaging of mRNA distribution in mouse embryonic neocortex,<sup>22</sup> while other approaches including mixed monolayers and streptavidin have been employed by other investigators.<sup>23,24</sup>

## EXPERIMENTAL SECTION

**Materials.** The cone-shape dendrons, 9-anthrylmethyl-3-(((tris((2-[[tris((2-carboxyethoxy)methyl)methyl]amino)carbonyl]ethoxy)methyl)methyl]amino)carbonyl)propyl)carbamate (or 9-acid) and 9-anthrylmethyl-3-(((tris((1-[[tris((2-[[tris((2-carboxyethoxy)methyl)methyl]amino)carbonyl]ethoxy)methyl]amino)carbonyl]2-ethoxy)methyl)methyl]amino)carbonyl)propyl)carbamate (or 27-acid) used in this work were prepared in this group.<sup>22</sup> The silane coupling reagent, (3-glycidoxypropyl)methyldiethoxysilane (GPDES), was purchased from Gelest, and all other chemicals for surface reactions were of reagent grade from Sigma-Aldrich. All washing solvents for the substrates and the probes were of HPLC grade from Mallinckrodt Baker. Ultrapure deionized water (18.2 MΩ·cm) was obtained from a Milli-Q purification system (Millipore). The polished prime Si(100) wafers (dopant, phosphorus; resistivity, 1.5–2.1 Ω·cm) were purchased from Silicon Quest International. The standard V-shaped silicon nitride probes (MSCT-AUNM) with five triangular and one rectangular cantilevers were purchased from Veeco Instruments, and a triangular cantilever of the smallest spring constant ( $k = \text{ca. } 10 \text{ pN/nm}$ ) was used.

**Preparation of Proteins.** GST-fused proteins, SH3 domain of PLC-γ1, Munc-18-1, and PX domain of PLD1, were prepared as described previously.<sup>25,26</sup> *Escherichia coli* (*E. coli*) BL21 cells were transformed with individual expression vectors encoding the GST-fused proteins and purified by a standard method which included lysing *E. coli* with a buffer containing 1% Triton X-100 and 1% cholic acid, centrifuging the lysate at 100 000g for 30 min at 4 °C, and separating with glutathione–Sepharose 4B.<sup>27</sup> Proteins were eluted three times by using 50 mM Tris/HCl buffer (pH 7.0) dissolving glutathione (10 mM) and dithiothreitol (1 mM) for 1 h at 4 °C. The GST protein fused to Munc-18-1 or SH3 domain of PLC-γ1 has been cleaved by thrombin and purified with gel filtration.

**Cleaning the Substrate and Probe.** Silicon wafers were immersed in piranha solution ( $\text{H}_2\text{SO}_4/30\% \text{H}_2\text{O}_2 = 7:3$  (v/v)) and sonicated for 4 h. Then, the substrates were heated in RCA I solution ( $\text{H}_2\text{O}/30\% \text{H}_2\text{O}_2/\text{NH}_4\text{OH} = 5:1:1$  (v/v/v)) and RCA II

- (13) Exton, J. H. *Biochim. Biophys. Acta* **1999**, *1439*, 121–133.  
 (14) Jang, I. H.; Lee, S.; Park, J. B.; Kim, J. H.; Lee, C. S.; Hur, E.-M.; Kim, I. S.; Kim, K.-T.; Yagisawa, H.; Suh, P.-G.; Ryu, S. H. *J. Biol. Chem.* **2003**, *278*, 18184–18190.  
 (15) Lee, H. Y.; Park, J. B.; Jang, I. H.; Chae, Y. C.; Kim, J. H.; Kim, I. S.; Suh, P.-G.; Ryu, S. H. *J. Biol. Chem.* **2004**, *279*, 16339–16348.  
 (16) Wang, Z.; Glück, S.; Zhang, L.; Morgan, M. F. *Mol. Cell. Biol.* **1998**, *18*, 590–597.  
 (17) Pei, Z.-D.; Williamson, J. R. *FEBS Lett.* **1998**, *423*, 53–56.  
 (18) Yu, H.; Fukami, K.; Itoh, T.; Takenawa, T. *Exp. Cell Res.* **1998**, *243*, 113–122.  
 (19) Hata, Y.; Slaughter, C. A.; Südhof, T. C. *Nature (London)* **1993**, *366*, 347–351.  
 (20) Pevsner, J.; Hsu, S. C.; Scheller, R. H. *Proc. Natl. Acad. Sci. U.S.A.* **1994**, *91*, 1445–1449.  
 (21) Garcia, E. P.; Gatti, E.; Butler, M.; Burton, J.; Camilli, P. D. *Proc. Natl. Acad. Sci. U.S.A.* **1994**, *91*, 2003–2007.

- (22) Jung, Y. J.; Park, Y. S.; Yoon, K.-J.; Kong, Y.-Y.; Park, J. W.; Nam, H. G. *Nucleic Acids Res.* **2009**, *37*, e10.  
 (23) Dupres, V.; Menozzi, F. D.; Loch, C.; Clare, B. H.; Abbott, N. L.; Curnot, S.; Bompard, C.; Raze, D.; Dufrière, Y. F. *Nat. Methods* **2005**, *2*, 515–520.  
 (24) Jin, Y.; Wang, K.; Tan, W.; Wu, P.; Wang, Q.; Huang, H.; Huang, S.; Tang, Z.; Guo, Q. *Anal. Chem.* **2004**, *76*, 5721–5725.  
 (25) Lee, S.; Park, J. B.; Kim, J. H.; Kim, Y.; Kim, J. H.; Shin, K. J.; Lee, J. S.; Ha, S. H.; Suh, P. G.; Ryu, S. H. *J. Biol. Chem.* **2001**, *276*, 28252–28260.  
 (26) Kim, J. H.; Lee, S.; Kim, J. H.; Lee, T. G.; Hirata, M.; Suh, P. G.; Ryu, S. H. *Biochemistry* **2002**, *41*, 3414–3421.  
 (27) Lee, C.; Kim, S. R.; Chung, J. K.; Frohman, M. A.; Kilimann, M. W.; Rhee, S. G. *J. Biol. Chem.* **2000**, *275*, 18751–18758.

solution ( $\text{H}_2\text{O}/30\% \text{H}_2\text{O}_2/\text{HCl} = 6:1:1$  (v/v/v)) at  $80^\circ\text{C}$  for 10 min, sequentially. Silicon nitride probes were first oxidized by heating in 10% nitric acid at  $80^\circ\text{C}$  for 20 min. The substrates and probes were washed and rinsed thoroughly with a copious amount of water. The clean substrates and the probes were dried in a vacuum chamber for 20 min and used immediately for the next steps.

**Preparing the Silane Surface.** The above clean wafers and the probes were placed in 20 mL of anhydrous toluene dissolving 0.20 mL GPDES under nitrogen atmosphere for 4 h. After the silylation, they were washed with toluene briefly and baked at  $110^\circ\text{C}$  for 30 min. The substrates were sonicated in toluene, toluene–methanol (1:1 (v/v)), and methanol each for 3 min in a sequential manner. The probes were rinsed thoroughly with toluene, and then with methanol. The substrates and the probes were dried in a vacuum chamber. The silanized substrates and the probes were heated in ethylene glycol solution with two drops of 95% sulfuric acid at  $90^\circ\text{C}$  for 8 h. After cooling, the substrates were sonicated in methanol, ethanol, and methanol each for 3 min in a sequential manner. The probes were rinsed thoroughly with ethanol, and then with methanol. The substrate and the probes were dried in a vacuum chamber.

**Preparing the Dendron-Modified Surface.** The substrates and the probes treated as in the above were placed in a methylene chloride solution with a small amount of dimethylformamide (DMF) dissolving the dendron (1.0 mM) and a coupling agent, 1,3-dicyclohexylcarbodiimide (DCC) (9.0 mM for 9-acid, 27 mM for 27-acid), in the presence of 4-dimethylaminopyridine (DMAP) (0.90 mM). After allowing 12 h, the substrates were sonicated in methylene chloride, methanol, and water each for 3 min in a sequential manner. The probes were rinsed thoroughly with methylene chloride, and then with methanol, last with water. The substrates and the probes were dried in a vacuum chamber. The dendron-modified substrates and probes were immersed into a methylene chloride solution dissolving trifluoroacetic acid (TFA) (1.0 M), and the solution was stirred for 3 h at room temperature. After the reaction, they were soaked in a methylene chloride solution dissolving diisopropylethylamine (DIPEA) (20% (v/v)) for 10 min. The substrates were sonicated in methylene chloride and methanol each for 3 min, and the probes were rinsed thoroughly with methylene chloride, and then with methanol. The substrates and the probes were dried in a vacuum chamber.

**Preparing the GSH-Modified Surface.** The resulting substrates and probes were placed in a 50 mM  $\text{NaHCO}_3$  buffer (pH 8.5) with a small amount of DMF dissolving *N*-(4-maleimidobutyric acid)hydroxysuccinimide ester (GMBS) (16 mM). After allowing 3 h, the substrates and the probes were rinsed thoroughly with water. The substrates and the probes were dried in a vacuum chamber. The substrates and the probes were immersed into a PBS buffer (10 mM phosphate buffer, 2.7 mM KCl, 137 mM NaCl, pH 7.4) dissolving GSH (16 mM) for 12 h. The substrates were sonicated in water for 3 min, and the probes were rinsed thoroughly with water. The substrates and probes were dried in a vacuum chamber. To block unreacted tethered GMBS, the substrates and the probes were immersed into a PBS buffer dissolving 2-mercaptoethanol (1.6 M), and the solution was stirred for 2 h at room temperature. The substrates were sonicated in water for 3 min,

and the probes were rinsed thoroughly with water. The substrates and the probes were dried in a vacuum chamber.

**Immobilization of Proteins on the Surface.** The substrates were placed in a PBS buffer dissolving GST-fused PX (0.43  $\mu\text{g}/\text{mL}$ ) at  $4^\circ\text{C}$  for 30 min, and the probes were placed in a PBS buffer dissolving GST-fused Munc-18-1 (0.95  $\mu\text{g}/\text{mL}$ ) or GST-fused SH3 (0.35  $\mu\text{g}/\text{mL}$ ) at the above condition. Finally, the substrates and the probes were rinsed thoroughly with a PBST buffer (10 mM phosphate buffer, 2.7 mM KCl, 137 mM NaCl, 0.1% Tween 20, pH 7.4). The substrates and the probes were stored in the PBS buffer at  $4^\circ\text{C}$ .

**AFM Measurements and Analysis.** Force–distance curves were obtained by using a NanoWizard AFM (JPK Instrument). All force measurements were performed in a liquid cell filled with freshly prepared PBS buffer at  $15^\circ\text{C}$ . The spring constant,  $k_c$ , of each individual probe was calibrated in solution before each run with the thermal fluctuation method available via a NanoWizard software. The spring constant of each resulting probe ranges between 10 and 14 pN/nm. The loading rate was varied by changing the retraction speed from 10 to 10 000 nm/s for each approach–retraction cycle while keeping the constant approach speed of 500 nm/s. The loading rate was calculated from the slope prior to the rupture event in force–distance curve and the retraction speed.<sup>10</sup> Force–distance curves corresponding to specific interactions only were used for data analysis. Such curves were distinguished from nonspecific force measurements due to the presence of nonlinear adhesion profiles in their retract traces, corresponding to extension of the biomolecular complex and/or dendron chemistry prior to the bond rupture event. Curves with linear adhesion profiles (with no extension) were attributed to nonspecific interactions between the underlying substrates and were not included. No additional data filtering was used to generate the histograms, and a bin size of 10 pN was chosen as this was the approximate level of noise within each force measurement (arising from thermal fluctuations of the cantilever). The most probable unbinding force was determined by fitting a Gaussian to the histogram of the force distribution. The median value of the Gaussian curve was taken as the most probable unbinding force. The unbinding probability was calculated from the ratio of the rupture events to the total measurements. The error in determining the median value was estimated by  $2\sigma/\sqrt{N}$ , where  $\sigma$  is the width of the distribution and  $N$  is the number of rupture events in the histogram.<sup>8</sup>

## RESULTS AND DISCUSSION

**Spacing on the Surface Generated by Dendrons.** To observe interaction between biomolecules at single molecular level, the surface modification technology for immobilization of biomolecules on the surface is important. In a previous study, we reported the ability of cone-shape dendron as a method of surface modification.<sup>11,22,28–34</sup> The strategy for measuring the specific

(28) Chio, Y.-S.; Yoon, C. M.; Lee, H. D.; Park, M.; Park, J. W. *Chem. Commun.* **2004**, *11*, 1316–1317.

(29) Hong, B. J.; Oh, S. J.; Youn, T. O.; Kwon, S. H.; Park, J. W. *Langmuir* **2005**, *21*, 4257–4261.

(30) Hong, B. J.; Sunkara, V.; Park, J. W. *Nucleic Acids Res.* **2005**, *33*, e106.

(31) Kwon, S. H.; Hong, B. J.; Park, H. Y.; Knoll, W.; Park, J. W. *J. Colloid Interface Sci.* **2007**, *308*, 325–331.

biomolecular interactions with the dendron-modified surface offers several advantages, as it allows regulation of the lateral spacing between biomolecules on surface. Because it is possible to preselect the size of the dendron, the realized spacing between pendent chemical functionalities at the dendron apexes is controllable. Also because the chemical backbone of the dendron can be tailored appropriately, electrostatic disturbance and nonspecific binding of biomolecules can be minimized while giving the immobilized molecule enhanced mobility.

In these studies to generate appropriate spacing of the proteins on the employed surfaces, either a dendron of the second generation, named 9-acid, or a dendron of the third generation, named 27-acid, was introduced onto the surfaces. After the deblocking the anthryl protection group in TFA, the surface was treated with GMBS to allow incorporation of thiol-terminated molecules. A tripeptide consisting of  $\gamma$ -glutamyl, cysteinyl, and glycyl group, GSH, was then immobilized on both substrates and AFM tips via the thiol functionality of the cysteine residue. Note that the carboxylate and amine group of the  $\gamma$ -glutamyl residue of GSH are the most important recognition sites for binding with GST, and the  $\gamma$ -glutamyl site is the major binding determinant.<sup>35,36</sup> The glycyl site is the least restrictive domain in the GSH-binding site of GST. Although it is also known that the thiol group of cysteinyl site is also important, our previous studies showed that GSH conjugated to controlled-pore glass beads through the cysteinyl group captured GST and GST-fused proteins reasonably well while suppressing nonspecific binding.<sup>37</sup> Finally, GST-fused Munc-18-1 was immobilized onto the generated GSH-tethered AFM tips, and GST-fused PX was bound to GSH-functionalized substrates via the GSH–GST interaction. In order to avoid decomposition of the proteins, the immobilization was carried out at 4 °C. The GSH–GST interaction of which the affinity is reasonably strong has been widely used for purifying proteins.<sup>27</sup> In addition, because GST can be fused at a selected site of a protein away from the binding domain, the activity for the binding remains intact for AFM studies.

In order to understand the effect of the dendron spacing, interaction forces between PX and Munc-18-1 were measured at a retraction speed of 500 nm/s with substrates and tips modified by either the 9-acid or 27-acid species. Also, because of the limited stability of the proteins at room temperature, all the force measurements were carried out at 15 °C. As shown in Figure 2, the obtained histograms of rupture forces were fitted with a single Gaussian curve, and the probability of observing no rupture events is noted (indicated by the arrow). To generate the force histogram, a whole set of the force–distance curves recorded was utilized, and for the small number of force–distance curves obtained with the multiple peaks (mostly with double peaks), the force corresponding to the last peak was incorporated. Although the prob-

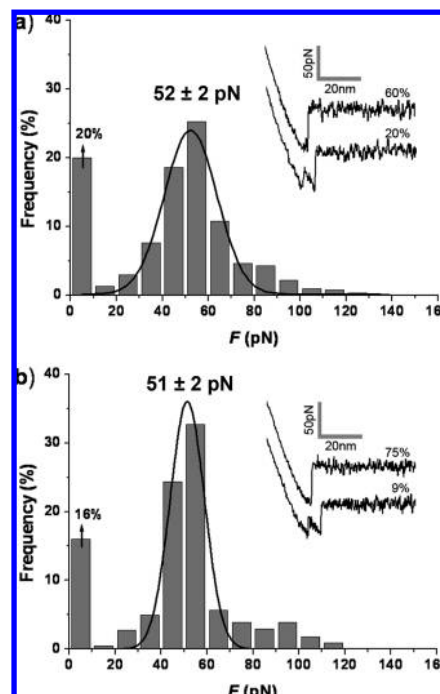


**Figure 2.** Measurement of the unbinding force between PX and Munc-18-1 with the dendron-modified surface at a retraction speed of 500 nm/s. Force–distance curves and force histogram were obtained by using 9-acid ( $n = 539$ ) (a) and 27-acid ( $n = 443$ ) (b). The value indicated by an arrow is the percentage of no unbinding events.

ability of the rupture event and the median rupture force were almost equal for the two surface immobilization methods, the sharpness of the histogram and the ratio between the force–distance curve with the single peak and the one with multiple peaks (mostly double peaks) were dependent on the dendron species employed. In the case of the 9-acid modification (Figure 2a), both curves with single peaks (top curve) and multiple peaks (bottom curve) were observed at a frequency of 60% and 20% of the measurements, respectively. The median rupture force was  $52 \pm 2$  pN, and the half-maximum width of the histogram was 23 pN. On the other hand, in the case of the 27-acid modification (Figure 2b), curves with single peaks (top curve) and multiple peaks (bottom curve) were observed at a frequency 75% and 9%, respectively. In this case the median rupture force was  $51 \pm 2$  pN, and the half-maximum width of the histogram was 15 pN. With the 27-acid modification, the histograms were sharper (23 vs 15 pN), and the ratio of the curves with single peaks to those with multiple peaks was 8.3:1, whereas it was 3.0:1 for the 9-acid.

While frequently single peaks have been taken into account for the histograms, we believed this was a good opportunity to see whether we ended up with an identical histogram or similar histograms regardless of AFM tip and substrate surface. For this end, additional histograms were also generated from the same data set, using only the curves with single peaks, i.e., excluding the curves with multiple peaks (Supporting Information). For both surface modification approaches, using the particular subsets did not improve the sharpness of the histograms. The histograms obtained with (27-acid)-modified surfaces were consistently sharper, compared with those prepared with the 9-acid, regardless of the data processing method to generate the histograms. These results indicate that employment of the 27-acid for large biomolecules,

- (32) Oh, S. J.; Ju, J.; Kim, B. C.; Ko, E.; Hong, B. J.; Park, J.-G.; Park, J. W.; Choi, K. Y. *Nucleic Acids Res.* **2005**, *33*, e90.  
(33) Hong, B. J.; Shim, J. Y.; Oh, S. J.; Park, J. W. *Langmuir* **2003**, *19*, 2357–2365.  
(34) Kim, J. S.; Jung, Y. J.; Park, J. W.; Shaller, A. D.; Wan, W.; Li, A. D. Q. *Adv. Mater.* **2009**, *21*, 786–789.  
(35) Adang, A. E. P.; Brussee, J.; Meyer, D. J.; Coles, B.; Ketterer, B.; Gen, A. V. D.; Mulder, G. J. *Biochem. J.* **1988**, *255*, 721–724.  
(36) Adang, A. E. P.; Brussee, J.; Gen, A. V. D.; Mulder, G. J. *Biochem. J.* **1990**, *269*, 47–54.  
(37) Chen, L.-H.; Choi, Y.-S.; Kwon, J.; Wang, R.-S.; Lee, T.; Ryu, S. H.; Park, J. W. *Tetrahedron* **2004**, *60*, 7293–7299.

or in other words, the use of a larger spacing, is more effective in realizing single rupture events.

High-resolution scanning electron microscopy showed that 9-acid generated a spacing of 3.2 nm in average, and the dendron surface binding also was confirmed by the absorption peak arising from the anthracene moiety of the unprotected dendron after the self-assembly.<sup>29</sup> With the use of this method the absorbance of 27-acid was found to be approximately half of that of 9-acid, giving an average spacing of 5 nm. The sharpening of the force distribution is an interesting part of the current study and was also reported in our previous studies of DNA interactions.<sup>11</sup> The sharpening of the distributions observed for 27-acid occurred simultaneously with a higher propensity of observing force measurements with single adhesion events. Both of these observations are consistent with a higher likelihood of recording single-molecule interaction events, and also the fact that the observed size of Munc-18-1 is  $7.0 \times 8.5 \text{ nm}^2$ <sup>38</sup> and the estimated diameters of SH3 and PX are around 3 nm suggests the larger spacing generated by 27-acid is more relevant. Within these studies, 27-acid would have a better performance than 9-acid, and this dendron species was therefore employed for the remaining experiments. However, the surface packing of the larger dendron species may result in a higher percentage of unfilled space (or vacancy) on the surface and/or larger are vacancies. This could result in a higher chance of recording undesirable nonspecific interactions originating from the underlying surface chemistry. While we are currently performing studies to investigate the precise origin (e.g., binding efficiency of protein, packing density of dendron, etc.) of these observations, it should be noted that in these studies the improved performance of the 27-acid surfaces was sufficient to justify its preferential use for the remaining experiments. It should also be noted that the probability of observing a rupture event when using the 27-acid was approximately 2-fold higher than typically observed when using other surface modification methods.<sup>23,39</sup> These results demonstrate the importance of appropriate spacing between biomolecules immobilized on a surface and the suitability of dendron-modified surfaces for the molecular-level recognition studies.

**Specificity of the PX–(Munc-18-1) Interaction.** We recorded force–distance curves while (Munc-18-1)-functionalized AFM probes were brought into and out of contact with PX-modified substrates. As mentioned above, rupture events were recorded at a frequency of 84% and mostly single peaks were observed. The median rupture force was  $51 \pm 2 \text{ pN}$ , and the half-maximum width of the histogram was 15 pN. Because independent measurements of the force between GSH and GST showed a force of  $92 \pm 2 \text{ pN}$  (Supporting Information), the observed measurements can be assigned to the rupture events between PX and Munc-18-1. To check the specificity of the measured interaction forces, we recorded force–distance curves in a solution containing 50 nM ( $3.4 \mu\text{g/mL}$ ) Munc-18-1. As shown in Figure 3a, the probability of the rupture event was found to decrease from 84% to 8%. For two additional control experiments in the absence of free Munc-18-1, the PX-modified substrate was replaced by a

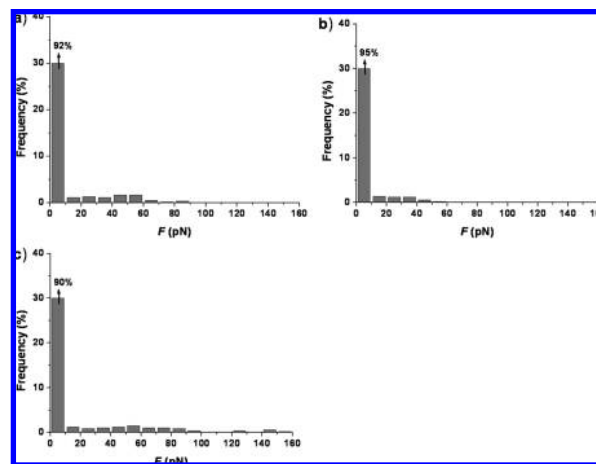


**Figure 3.** Measurement of the specificity of PX–(Munc-18-1) interaction with the (27-acid)-modified surface. (a) Force histogram ( $n = 544$ ) obtained in the presence of 50 nM ( $3.4 \mu\text{g/mL}$ ) Munc-18-1. (b) Force histogram ( $n = 501$ ) obtained by using a BSA substrate. (c) Force histogram ( $n = 482$ ) obtained by using a GSH substrate. The value indicated by an arrow is the percentage of no unbinding events.

bovine serum albumin (BSA)-coated substrate, where BSA was linked to the dendron-modified substrate using di(*N*-succinimidyl)carbonate (DSC). As in Figure 3b, almost no rupture events were detected. A GSH-tethered substrate without PX immobilization was examined. Figure 3c shows that the result is almost the same to the other two controls except for the presence of a small number of large forces (over 100 pN), possibly associated with the small size of the GSH tripeptide which is not capable of blocking the interaction with the underlying surface. To reconfirm the single interactions between PX and Munc-18-1, we measured the unbinding force at reduced surface density of the immobilized proteins on the AFM tip and substrate surface. Although the chance of finding points showing the specific interaction reduced, the median force values were consistently between 49 and 51 pN at these points (Supporting Information). The above results support that the initially measured interaction is attributable to the specific PX–(Munc-18-1) interaction.

To investigate the stability of the immobilized proteins at 15 °C, we also followed the PX–(Munc-18-1) interaction over time. Although the mean specific interaction force remained constant for 4 h after starting of the force measurement, after this time the unbinding force was found to reduce (Supporting Information). This result indicates that the proteins denatured or decomposed after 4 h under the employed conditions. Because of this limitation, all force measurements were thus performed in less than 4 h, and new tips and substrates prepared in the same batch were employed for further measurements.

#### Interaction Force between the PX–SH3 Pair.

Force–distance curves were recorded to investigate the interaction between PX and SH3. As previously, the (27-acid)-modified tip was functionalized with GST-fused SH3 through the GSH–GST interaction, and GST-fused PX was immobilized on the substrate treated in the same way. As shown in Figure 4a, the unbinding force histogram was fitted with a single Gaussian curve, in which the median rupture force was  $42 \pm 2 \text{ pN}$ , the half-maximum width of the histogram was 17 pN, and the probability of observing no unbinding events was 23%. As shown in the inset, both curves

(38) Misura, K. M. S.; Scheller, R. H.; Weis, W. I. *Nature (London)* **2000**, *404*, 355–362.

(39) Eckel, R.; Wilking, S. D.; Becker, A.; Sewald, N.; Ros, R.; Anselmetti, D. *Angew. Chem., Int. Ed.* **2005**, *44*, 3921–3924.

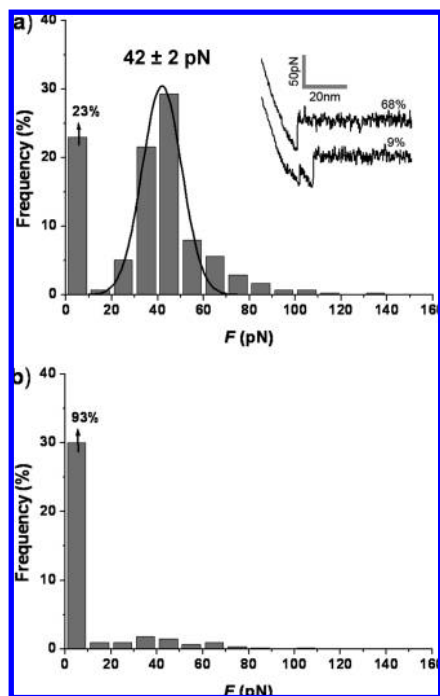


**Figure 4.** Measurement of the unbinding force between PX and SH3 with the (27-acid)-modified surface. (a) Force–distance curves and force histogram ( $n = 413$ ) of the specific interaction. (b) Force histogram ( $n = 548$ ) obtained in the presence of 100 nM ( $1.0 \mu\text{g/mL}$ ) SH3. The value indicated by an arrow is the percentage of no unbinding events.

with single peaks (top curve) and with multiple peaks (bottom curve) were observed at a frequency of 68% and 9%, respectively (ratio, 7.8:1). Rupture force histograms were generated using the whole set of the force–distance curves recorded, and for the force–distance curves with the multiple peaks again the force corresponding to the last peak was utilized. As in Figure 4b, the specificity of the measured interaction was confirmed by adding free SH3 in solution. In the presence of 100 nM ( $1.0 \mu\text{g/mL}$ ) SH3, the probability of observing a rupture event reduced from 77% to 7%. These results indicate that the above-measured unbinding force can be attributed to the specific PX–SH3 interaction.

Additionally, we measured the interaction between Munc-18-1 and SH3 (Supporting Information). The low probability (<4%) of the unbinding event confirms that there is no specific interaction between Munc-18-1 and SH3. This behavior is reminiscent of that observed for the control experiments (Figure 3) and indicates that interaction between Munc-18-1 and PLC- $\gamma$ 1 is insignificant in comparison to the other two receptor–ligand pairs.

**Dynamics of the Interaction between the Proteins.** To understand the dissociation mechanism of the protein pairs, we performed dynamic force spectroscopy (DFS) experiments for the PX–(Munc-18-1) and PX–SH3 interaction at 15 °C. Specifically, we measured the dependence of the unbinding force on the applied loading rate and plotted the unbinding forces against the logarithm ( $\ln(r)$ ) of the loading rate (Figure 5). Upon changing the retraction speed from 10 to 10 000 nm/s, it was observed that the unbinding force increased linearly with the  $\ln(r)$ , and the data were fitted with a straight line for respective protein pairs, reflecting the presence of one potential barrier in the energy

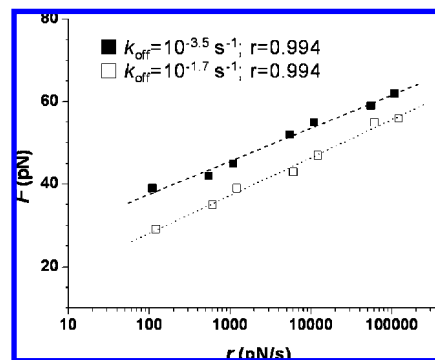


**Figure 5.** Dependence of the unbinding forces on the logarithm of the loading rate for PX–(Munc-18-1) (■) and PX–SH3 (□) interaction.

landscape from the DFS analysis.<sup>40</sup> This observation is reminiscent of other proteins that show an linear increase of the unbinding force with the logarithm of the loading rate.<sup>10,39,41</sup> The unbinding force ( $F$ ) is given by

$$F = \frac{k_B T}{x_\beta} \ln \left( \frac{r x_\beta}{k_{\text{off}} k_B T} \right) \quad (1)$$

where  $k_B$  is the Boltzmann constant and  $T$  is the absolute temperature.<sup>42</sup> By applying eq 1 to our experimental data we were able to determine two important kinetic parameters for the interactions investigated; the length scale of potential barriers on the dissociation pathway,  $x_\beta$ , and the kinetic off-rate constant for the dissociation,  $k_{\text{off}}$  (at zero force). The slope,  $k_B T/x_\beta$ , obtained by plotting  $F$  as a function of  $\ln(r)$  in these experiments resulted in  $x_\beta = 1.2 \pm 0.1$  nm for PX–(Munc-18-1) and  $1.0 \pm 0.1$  nm for PX–SH3. The length scale,  $x_\beta$ , is the distance from a bound state to the transition state along the reaction coordinate in the energy landscape and represents the projected bond displacement along the direction of the applied force. The obtained values are in the range of the length scale for other proteins.<sup>39,40,42</sup> Extrapolation of the data to the loading rate at zero force,  $F = 0$ , allows estimation of the dissociation rate constant ( $k_{\text{off}} = r x_\beta / k_B T$ ) for the potential barrier, yielding kinetic off-rate constants for PX–(Munc-18-1) and PX–SH3, respectively, of  $10^{-3.4 \pm 0.3} \text{ s}^{-1}$  and  $10^{-1.7 \pm 0.1} \text{ s}^{-1}$ . The resulting values are in the range of the published off-rate constants for other signal-transducing proteins.<sup>43–45</sup> Because independent force measurement of the GST–GSH pair upon the loading rate showed a different slope, and  $x_\beta$  and  $k_{\text{off}}$  values compared with those obtained for PX–(Munc-18-1) and PX–SH3 pairs, it is safe to say that rupture of the GST–GSH interaction was not involved in the measurements for the former two pairs (Supporting Information). For each of PX–(Munc-18-1) and PX–SH3 pair, three independent experiments were conducted

(40) Merkel, R.; Nassoy, P.; Leung, A.; Ritchie, K.; Evans, E. *Nature (London)* **1999**, *397*, 50–53.

(41) Yersin, A.; Hirling, H.; Steiner, P.; Magnin, S.; Regazzi, R.; Hüni, B.; Huguenot, P.; Rios, D. L.; Dietler, G.; Catsicas, S.; Kasas, S. *Proc. Natl. Acad. Sci. U.S.A.* **2003**, *100*, 8736–8741.

(42) Evans, E.; Ritchie, K. *Biophys. J.* **1997**, *72*, 1541–1555.

(43) Runnels, L. W.; Scarlata, S. F. *Biochemistry* **1998**, *37*, 15563–15574.

(44) Pabst, S.; Margittai, M.; Vainius, D.; Langen, R.; Jahn, R.; Fasshauer, D. *J. Biol. Chem.* **2002**, *277*, 7838–7848.

(45) Fasshauer, D.; Antonin, W.; Subramaniam, V.; Jahn, R. *Nat. Struct. Biol.* **2002**, *9*, 144–151.

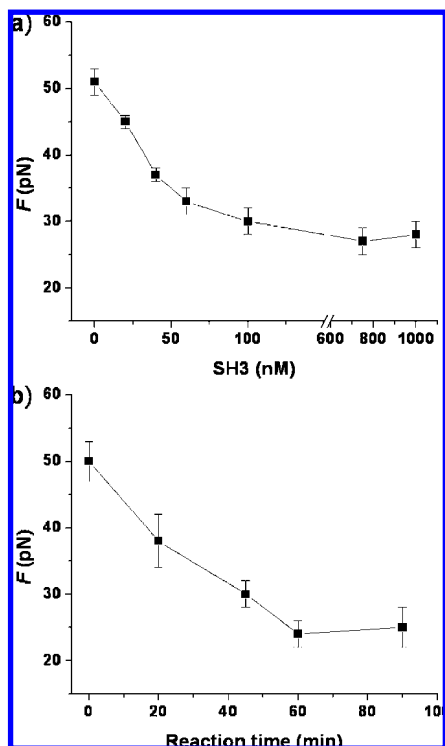


**Figure 6.** Modulation of the PX-(Munc-18-1) interaction with SH3. (a) Change of the interaction between PX and Munc-18-1 upon addition of SH3. The unbinding force obtained for each concentration of SH3 is the median force from Gaussian fits to the force histograms for all values measured at various positions on a substrate. The values acquired after allowing sufficient reaction time (60 min) were incorporated. (b) The change in median force as a function of reaction time obtained in the presence of 100 nM (1.0  $\mu\text{g/mL}$ ) SH3. The forces in panels a and b correspond to the median value of the Gaussian fits to the histogram, with each error bar being the standard deviation.

using new tips and substrates. For both cases fairly good fits to the linearity were observed. The observed  $k_{\text{off}}$  values were  $10^{-3.5} \text{ s}^{-1}$  (correlation coefficient  $r = 0.994$ ),  $10^{-3.1} \text{ s}^{-1}$  ( $r = 0.994$ ), and  $10^{-3.6} \text{ s}^{-1}$  ( $r = 0.983$ ) for PX-(Munc-18-1), and  $10^{-1.9} \text{ s}^{-1}$  ( $r = 0.991$ ),  $10^{-1.6} \text{ s}^{-1}$  ( $r = 0.985$ ), and  $10^{-1.7} \text{ s}^{-1}$  ( $r = 0.994$ ) for PX-SH3. Figure 5 shows two representative plots. Although the retraction speed was set to fixed values at each set of the experiments, the loading rate varied slightly due to different spring constants. Therefore, the values obtained through three different experiments were averaged to determine the  $k_{\text{off}}$  and  $x_{\beta}$  value. It should be noted that the accuracy of the  $k_{\text{off}}$  value is highly dependent upon the standard deviation of the intercept (typically 10–20% of the measured value in these particular cases), and thus obtaining data with a strict linear dependence of which a correlation coefficient is close to unity is of utmost importance.

#### Modulation of the PX-(Munc-18-1) Interaction with SH3.

To investigate the influence of PLC- $\gamma$ 1, which is known as a competing protein of Munc-18-1,<sup>15</sup> on the PLD1-(Munc-18-1) interaction, the unbinding forces between PX and Munc-18-1 were measured in the presence of various SH3 concentrations (20, 40, 60, and 100 nM and 0.75 and 1.0  $\mu\text{M}$ ) (Figure 6a). This study is reminiscent of the force titration recorded by Vezenov et al. and Smith et al. who changed pH to probe the interaction between

chemical functional groups.<sup>46,47</sup> After injection of SH3, the interaction was measured at a position of the substrate as a function of time. In the presence of 100 nM (1.0  $\mu\text{g/mL}$ ) SH3, the unbinding force decreased gradually with the reaction time and the end point was reached in 60 min (Figure 6b). In addition, it was observed that the reaction time required for reaching the end point was almost constant at various concentrations.

Rather than observing an abrupt drop in the frequency of observing an interaction (i.e., as for the controls presented in Figure 3), a gradual drop in the magnitude of the median recorded force was observed for these experiments. To explain this behavior we hypothesize that on binding SH3 the PX domain undergoes a change in structure, such that the Munc-18-1 binding site becomes modified. While this is worthy of future investigation, it should also be noted that these observations may also arise from the differences between the conditions in these experiments and those within a live cell. Our in vitro examinations were carried out in the absence of the membrane, and the low temperature (15  $^{\circ}\text{C}$ ) utilized would slow down the reorganization rate. Because of instability of the isolated proteins at 37  $^{\circ}\text{C}$ , the rate of the conversion at the temperature could not be investigated. The observed data suggest that the binding of SH3 to PX domain initiates the rate-determining process, i.e., reorganization of PX domain, resulting in weakening of the force between PX and Munc-18-1. The fast binding of SH3 to the PX domain is supported by the effective measurement of the force between the immobilized pairs (Figure 4a). The estimated contact time between PX and Munc-18-1 during the cycle of the employed force measurement is on the time scale of 0.15 s.

Comparison of the force histograms recorded at several lateral positions on the sample surface also gave additional information. The native conformation refers to the PX domain in the absence of SH3, and binding of SH3 only occurs after EGF treatment in the cell.<sup>14</sup> The force was measured at six different positions after allowing sufficient reaction time (60 min) for the reorganization of the PX domain induced by binding of SH3. At 100 nM of SH3, for five out of the six positions the median rupture forces were between 24 and 27 pN, but at one position a median force of 50 pN, equal to that recorded previously for PX-(Munc-18-1) in the absence of SH3, was observed (e.g., equivalent to the native state) (Supporting Information). We suggest that the lower forces are associated with the PX domain with a structure modified through SH3 binding, such that the Munc-18-1 binding site is changed. With reducing SH3 concentration the average force increased. To generate the histograms and identify the median force value at each concentration of SH3, the force values observed at all the locations at the sample surface were grouped together. As evident in the resulting titration curve (Figure 6a), the average unbinding force decreased gradually as the concentration of SH3 increased before saturating over 100 nM.

#### Modulation of the PX-SH3 Interaction with Munc-18-1.

To understand the modulation by Munc-18-1, a competing protein of PLC- $\gamma$ 1 in the PLD1-(PLC- $\gamma$ 1) interaction,<sup>15</sup> the unbinding forces between PX and SH3 were measured in solutions containing

(46) Vezenov, D. V.; Noy, A.; Rozsnyai, L. F.; Lieber, C. M. *J. Am. Chem. Soc.* **1997**, *119*, 2006–2015.

(47) Smith, D. A.; Mark, L. W.; Zhang, J.; Kirkham, J.; Robinson, C.; Marsh, A.; Wong, M. *J. Phys. Chem. B* **2000**, *104*, 8862–8870.

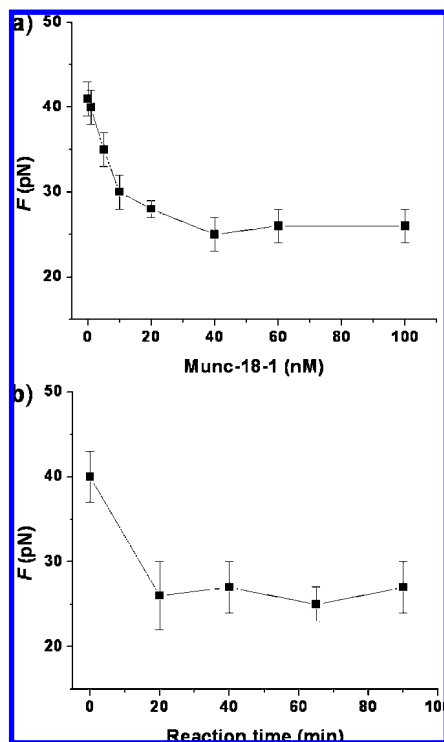


**Figure 7.** Modulation of the PX-SH3 interaction with Munc-18-1. (a) Change of the interaction between PX and SH3 upon adding Munc-18-1. The unbinding force obtained for each concentration of Munc-18-1 is the median force from Gaussian fits to the force histograms for all values measured at various positions on a substrate. The values acquired after allowing sufficient reaction time (60 min) were incorporated. (b) The change in force as a function of reaction time obtained in the presence of 100 nM (6.7  $\mu\text{g/mL}$ ) Munc-18-1. The forces in panels a and b are the median values determined from Gaussian fits of the histograms, and each error bar is the standard deviation.

Munc-18-1 of 1.0, 5.0, 10, 20, 40, 60, and 100 nM (Figure 7a). After injection of Munc-18-1, the interaction was measured at a position of the substrate as a function of time. In the presence of 100 nM (6.7  $\mu\text{g/mL}$ ) Munc-18-1, the unbinding force was found to decrease with the reaction time, and the end point was reached in 20 min (Figure 7b). The reaction time required for reaching the end point was almost constant at various concentrations. We also hypothesize that on binding Munc-18-1 the PX domain undergoes a change in structure, such that the SH3 binding site becomes modified. The observed result suggests that the binding of Munc-18-1 to PX domain is not a slow step in the employed conditions and that the Munc-18-1 binding also initiates a slow reorganization of the PX domain, resulting in a weakening of the force between PX and SH3. The reorganization of PX domain induced by binding of Munc-18-1 appeared to be faster than the previous modulation induced by SH3 binding. The fast binding of Munc-18-1 to PX domain was again supported by effective measurement of the force between the immobilized pairs (Figure 2b). The estimated contact time between PX and SH3 during a cycle of the force measurement is in the time scale of 0.15 s.

The forces were again measured at seven different locations on the substrate surface after the sufficient reaction time (60 min) for the reorganization of the PX domain induced by binding of Munc-18-1 was allowed. At 20 nM of Munc-18-1, for six out of seven positions the median forces were between 25 and 28 pN,

the median force value of 41 pN seen for the PX-SH3 interaction, equivalent to the situation prior to Munc-18-1 application, was observed at only one position (Supporting Information). We also suggest that the lower force values are attributed from a PX domain with a structure modified through Munc-18-1 binding, such that the SH3 binding site is changed. With decreasing concentrations of Munc-18-1, the average force recorded increased. Again, to generate the force histograms and identify the median force value at each concentration of Munc-18-1, the force values measured at all substrate locations were grouped together. As evident in the resulting titration curve (Figure 7a), the average unbinding force decreased gradually as the concentration of Munc-18-1 increased before saturating over 20 nM.

**Titration Curves.** The modulation of the median force in the presence of a competing protein, SH3 or Munc-18-1, (Figures 6a and 7a) suggests that AFM is able to provide information about thermodynamic characteristics. In this scheme, the immobilized Munc-18-1 is a probe monitoring the change (or reorganization) of its PX domain upon the binding of SH3. By taking the force values at various positions on the substrate the ratio between the SH3-bound PX and the free PX can be measured, and the ratio determines the median force from the entire measurements. Because the particular median force is a function of the equilibrium ratio, treatment of the titration curve will give an idea about the equilibrium behavior between PX and SH3. In the same way, the corresponding information for the PX and Munc-18-1 pair can be obtained with the SH3 probe. The above two titrations are special examples of the blocking experiments, as the force decreases not by the direct blocking but the conformational change induced by the binding of the neighboring site.

The number of positions in which the competing protein bound to PX domain on the substrate increases as the concentration of the competing protein increases. Consequently, the average force ( $\bar{F}(c_0)$ ) measured can be given as

$$\bar{F}(c_0) = (1 - \Phi)\bar{F}_i + \Phi\bar{F}_f \quad (2)$$

where  $c_0$  is the concentration of the competing protein,  $\bar{F}_i$  is average force measured for the bare interaction,  $\bar{F}_f$  is the average force measured at full saturation of the competing protein, and  $\Phi$  is the fraction of the competing protein bound positions over the total positions, assumed to be

$$\Phi(c_0) = \frac{c_0 K_A}{1 + c_0 K_A} \quad (3)$$

where  $K_A$  is the association constant. Combining eqs 2 and 3 gives

$$\frac{\bar{F}_i - \bar{F}(c_0)}{\bar{F}(c_0) - \bar{F}_f} = K_A c_0 \quad (4)$$

As shown in Figure 8, a plot of  $(\bar{F}_i - \bar{F}(c_0))/(\bar{F}(c_0) - \bar{F}_f)$  as a function of  $c_0$  yields a linear expression from which  $K_A$  can be calculated. The association constant at 15  $^\circ\text{C}$  obtained from this plot was  $(4.9 \pm 1.4) \times 10^7 \text{ M}^{-1}$  for the PX-SH3 pair, and it was  $(1.7 \pm 0.8) \times 10^8 \text{ M}^{-1}$  for the PX-(Munc-18-1) pair. The higher association constant for the latter pair seems to be in line with the larger force between the pair. The values measured here are in the range of the ones obtained for other

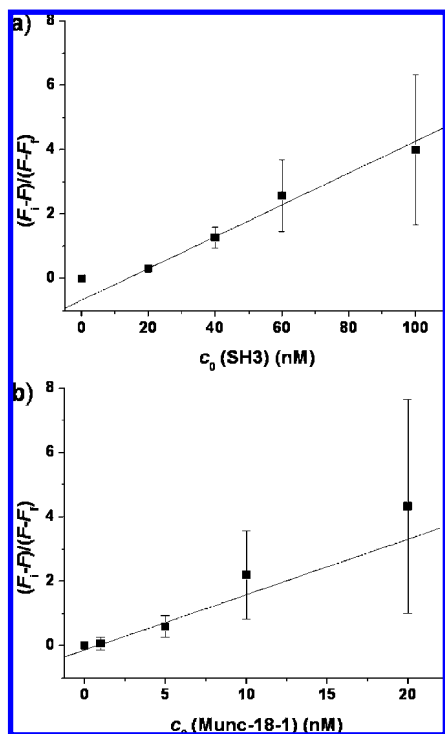


**Figure 8.** Measurement of the equilibrium affinity for PX–SH3 (a) and PX–(Munc-18-1) (b) interaction.  $(F_1 - F_0)/(F_0 - F_1)$  is plotted as a function of the concentration ( $c_0$ ) of SH3 (a) and Munc-18-1 (b).

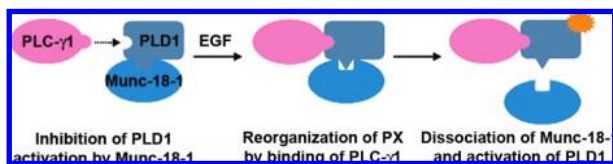


**Figure 9.** Proposed mechanism for the signal pathway.

signal-transducing proteins through other methodologies such as fluorescence spectroscopy.<sup>43,44,48</sup>

**Proposed Mechanism of Signal Pathway.** The dissociation of PLD–(Munc-18-1) and the association of PLD–(PLC- $\gamma$ 1) in vivo are induced by EGF stimulation.<sup>14,15</sup> Although both processes of protein pairs are induced by the same ligand, it is not presently clear whether the binding of PLC- $\gamma$ 1 induces the dissociation of Munc-18-1 directly. We observed that the interaction between PX and Munc-18-1 decreased in the presence of SH3 and that the PX domain reorganized itself within 1 h upon the binding of SH3. Also, the interaction between PX and SH3 was elucidated, whereas the interaction between Munc-18-1 and SH3 was not significant. Considering the additional information on the two different binding

sites for PLC- $\gamma$ 1 and Munc-18-1,<sup>14,15</sup> we are now ready to suggest a combined mechanism for the signal pathway. It is very likely that the reorganization of the PX domain of PLD1 occurs when PLC- $\gamma$ 1 binds to PX domain by EGF stimulation in cell signaling; subsequently, Munc-18-1, bound to PX domain of PLD1 to inhibit the activation of PLD1, dissociates allowing PLD1 to finally become activated for various cellular physiologies. A whole scheme of the proposed mechanism for the signal pathway is shown in Figure 9.

## CONCLUSION

The results presented in this study demonstrate that AFM is an excellent tool for elucidating the molecular behavior of signal-transducing protein pairs—PLD1/Munc-18-1/PLC- $\gamma$ 1. To enhance our ability to explore the recognition processes of protein pairs at the single molecular level, we have demonstrated that control of the lateral spacing between the proteins immobilized on surface is important. Specifically, we demonstrated efficacy of the cone-shape dendrons, in particular 27-acid, to improve the recognition efficiency and sharpen the obtained rupture–force histograms. The zero-force dissociation rate constants of the protein pairs at the single-molecule level were also estimated, and the titration curves provided information on the binding efficiency of the competing proteins. Although there are alternative conventional methodologies for obtaining such data, the ability to access them at the single molecular level, to retrieve the additional information on the energy landscape, and to observe the rate of PLD1 reorganization upon the binding of a competing protein are unique, and through this study, we were able to suggest a combined mechanism for the particular signal pathway. The study shows that AFM can be widely employed to elucidate protein–protein interactions and suggests that a new approach utilizing AFM for screening drug candidates would be feasible under a proper configuration.

## ACKNOWLEDGMENT

J.W.P. acknowledges financial support from an NCRC Grant funded by the Korean government (MEST) (R15-2004-033-06001-0), a Grant of the National R&D Program for Cancer Control, Ministry of Health & Welfare (0620200), and the Brain Korea 21 program. S.H.R. and J.W.P. thank a R&D Program for Fusion Strategy of Advanced Technologies (MKE).

## SUPPORTING INFORMATION AVAILABLE

Additional information as noted in text. This material is available free of charge via the Internet at <http://pubs.acs.org>.

Received for review November 18, 2008. Accepted March 5, 2009.

AC8024366

(48) Kusner, D. J.; Barton, J. A.; Qin, C.; Wang, X.; Iyer, S. S. *Arch. Biochem. Biophys.* 2003, 412, 231–241.